

# Dark Matter at the Fermi Scale

Jonathan L. Feng

*Department of Physics and Astronomy,  
University of California, Irvine, CA 92697, USA*

## Abstract

Recent breakthroughs in cosmology reveal that a quarter of the Universe is composed of dark matter, but the microscopic identity of dark matter remains a deep mystery. I review recent progress in resolving this puzzle, focusing on two well-motivated classes of dark matter candidates: WIMPs and superWIMPs. These possibilities have similar motivations: they exist in the same well-motivated particle physics models, the observed dark matter relic density emerges naturally, and dark matter particles have mass around 100 GeV, the energy scale identified as interesting over 70 years ago by Fermi. At the same time, they have widely varying implications for direct and indirect dark matter searches, particle colliders, Big Bang nucleosynthesis, the cosmic microwave background, and halo profiles and structure formation. If WIMPs or superWIMPs are a significant component of dark matter, we will soon be entering a golden era in which dark matter will be studied through diverse probes at the interface of particle physics, astroparticle physics, and cosmology. I outline a program of dark matter studies for each of these scenarios, and discuss the prospects for identifying dark matter in the coming years.

PACS numbers: 95.35.+d, 13.85.-t, 12.60.Jv, 04.65.+e

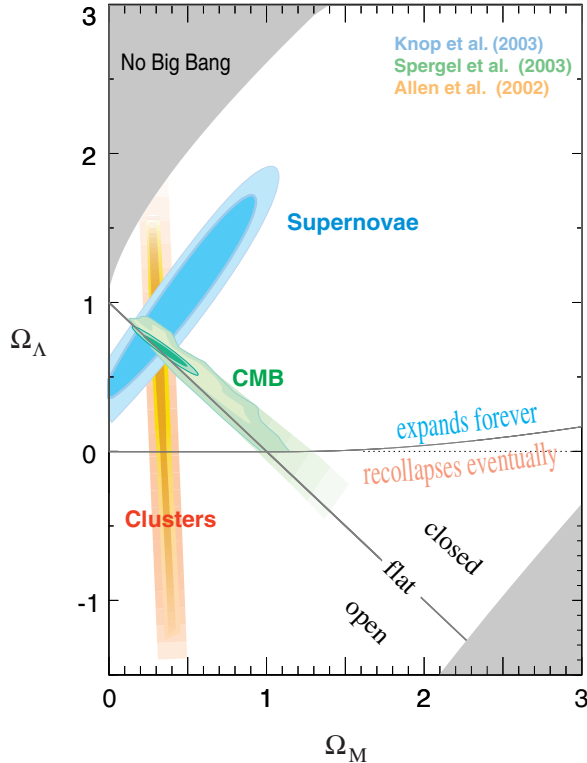


FIG. 1: Constraints on  $\Omega_M$  and  $\Omega_\Lambda$  from observations of supernovae, the CMB, and galaxy clusters [1].

## I. INTRODUCTION

In recent years, there has been tremendous progress in understanding the Universe on the largest scales. Observations of supernovae, the cosmic microwave background (CMB), and galaxy clusters have provided three stringent constraints on  $\Omega_M$  and  $\Omega_\Lambda$ , the energy densities of matter and dark energy in units of the critical density. These results are consistent and favor  $(\Omega_M, \Omega_\Lambda) \approx (0.3, 0.7)$ , as shown in Fig. 1. The amount of matter in the form of baryons is also constrained, both by the CMB and by the observed abundances of light elements together with the theory of Big Bang nucleosynthesis (BBN). Although there are at present possibly significant disagreements within the BBN data, the CMB and BBN data taken as a whole are also impressively consistent, providing yet another success for the current standard model of cosmology.

Through these and many other observations, the total energy densities of non-baryonic dark matter, baryons, and dark energy are constrained to be [2, 3]

$$\Omega_{\text{DM}} = 23\% \pm 4\% \quad (1)$$

$$\Omega_B = 4\% \pm 0.4\% \quad (2)$$

$$\Omega_\Lambda = 73\% \pm 4\% . \quad (3)$$

These results are remarkable. At least two of the constraints of Fig. 1 must be wrong to change the conclusions about the central values of  $\Omega_M$  and  $\Omega_\Lambda$ . These results are also remarkably precise — the fractional uncertainties on all three are  $\mathcal{O}(10\%)$ . Given that just a decade ago the range  $0.2 \lesssim \Omega_{\text{DM}} \lesssim 0.6$  was allowed and  $\Omega_\Lambda = 0$  was often assumed,

this represents spectacular progress. Although much of cosmology remains imprecise, as we will see, the quantum leap in precision in these three quantities already has dramatic implications for particle physics.

At the same time, recent progress in cosmology is probably best viewed as the first steps on the road to understanding the Universe. Consider an historical precedent: in 200 B.C., Eratosthenes determined the size of the Earth. On a day when the Sun was directly overhead in Syene, Eratosthenes sent a graduate student to measure the lengths of shadows in Alexandria. He was then able to extrapolate from the known distance between these two cities to determine the circumference of the Earth. His answer was

$$2\pi R_{\oplus} = 250,000 \text{ stadia} . \quad (4)$$

This result is remarkable. At the time of publication, it was bigger than many expected, leading many to be skeptical and helping to earn Eratosthenes the nickname “Beta” [4]. His result was also remarkably precise. We now know that it was good to less than 10% [5, 6, 7], where the leading source of uncertainty is systematic error from the exact definition of the unit “stadion” [8]. At the same time, the achievement of Eratosthenes, though important, could hardly be characterized as a complete understanding of the Earth. Rather, it was just the beginning of centuries of exploration, which eventually led to the mapping of continents and oceans, giving us the picture of the Earth we have today.

In a similar vein, recent breakthroughs in cosmology answer many questions, but highlight even more. Focusing on dark matter, the primary subject of this review, these include

- What particles form dark matter?
- Is dark matter composed of one particle species or many?
- What are dark matter’s spin and other quantum numbers?
- What are its interactions?
- How and when was it produced?
- Why does  $\Omega_{\text{DM}}$  have the observed value?
- How is dark matter distributed now?
- What is its role in structure formation?
- Is it absolutely stable?

Although these questions will continue to be sharpened by astrophysical observations at large length scales, it is clear that satisfying answers will require fundamental progress in our understanding of microphysics. This is nothing new — the history of advances in cosmology is to a large extent the story of successful synergy between studies of the Universe on the smallest and largest length scales. This interplay is shown in Fig. 2, where several milestones in particle physics and cosmology are placed along the cosmological timeline. As particle experiments reach smaller length scales and higher energies, they probe times closer to the Big Bang. Just as atomic physics is required to interpret the CMB signal from  $t \sim 10^{13}$  s after the Big Bang and nuclear physics is required to extrapolate back to BBN at  $t \sim 1$  s, particle physics, and particularly the physics of the weak or Fermi scale, is required to understand the era before  $t \sim 10^{-8}$  s, the era that contains the answers to many of our most basic questions.

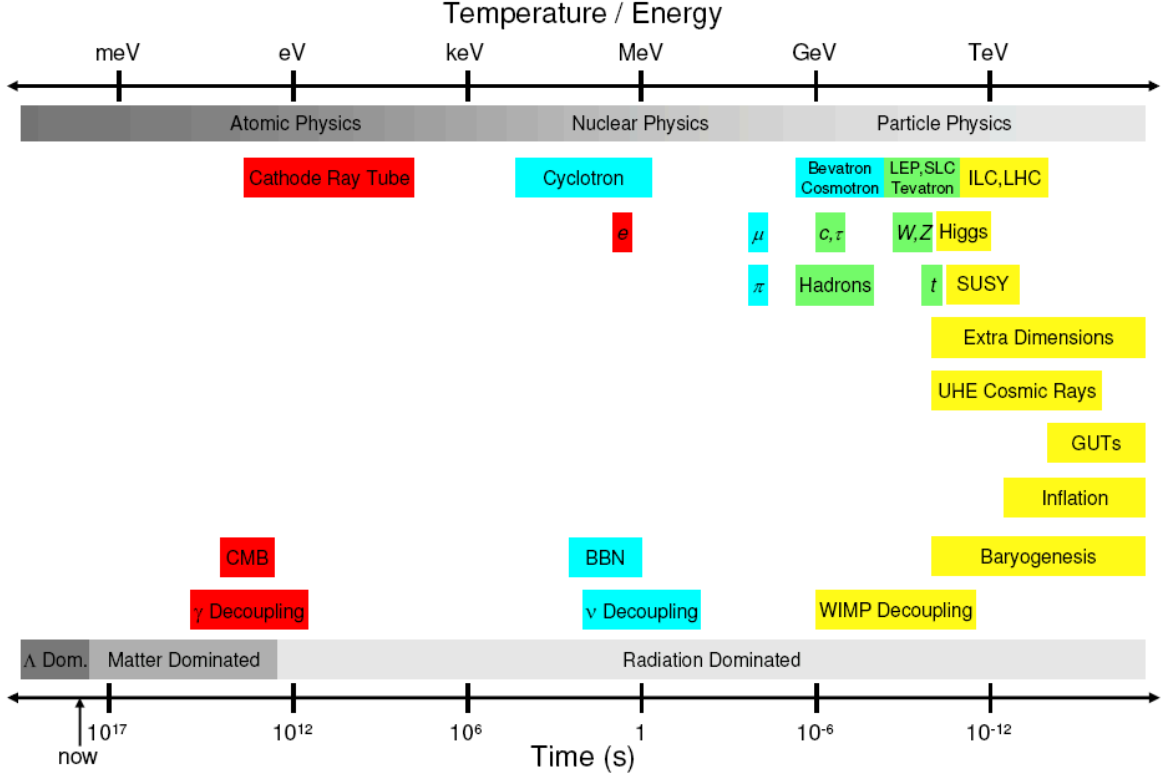


FIG. 2: Milestones in particle physics and cosmology along the cosmological timeline.

Here I will review recent progress in dark matter, focusing on new proposals for and studies of dark matter at the Fermi scale

$$M_F \sim 100 \text{ GeV} . \quad (5)$$

$M_F$  is the scale of the weak interactions; its importance for particle physics was realized by Fermi some 70 years ago. Remarkably, it is now appreciated that incisive studies of this scale may also yield deep insights into the dark matter problem as well. In the next few years, the Tevatron and Large Hadron Collider (LHC) will play the crucial role of opening the door to the Fermi scale. These will be followed, we hope, by detailed studies of new physics at these colliders and the proposed International Linear Collider (ILC). If dark matter particles do in fact have masses at the Fermi scale, these colliders, in conjunction with cosmological and astroparticle probes, will be essential for studying dark matter and unveiling its identity.

I begin with a review of the motivations to consider dark matter candidates with Fermi scale masses. These candidates may be divided into two classes: WIMPs and superWIMPs. I consider these in turn, discussing the basic scenarios, their implications for particle physics and cosmology, and the prospects for identifying dark matter and answering many of the other questions listed above. Further background and discussion on both these and other dark matter topics may be found in Refs. [9].

## II. WHY THE FERMI SCALE?

The particle or particles that make up most of dark matter must be stable, at least on cosmological time scales, and non-baryonic, so that they do not disrupt the successes of BBN. They must also be cold or warm to properly seed structure formation, and their interactions with normal matter must be weak enough to avoid violating current bounds from dark matter searches. The stringency of these criteria pale in comparison with the unbridled enthusiasm of theorists, who have proposed scores of viable candidates with masses and interaction cross sections varying over tens of orders of magnitude. In roughly the order in which they were proposed, these include axions [10, 11, 12], thermally-produced gravitinos [13, 14, 15, 16, 17, 18, 19, 20], neutralinos [21, 22], axinos [23], Q balls [24], wimpzillas [25], self-interacting dark matter [26], annihilating dark matter [27], Kaluza-Klein dark matter [28, 29], branons [30, 31], superWIMPs [32, 33], and many others.

Candidates with Fermi scale masses have received much of the attention, however. There are at least four good reasons for this. First, these proposals are testable. Second, new particles at the Fermi scale are independently motivated by attempts to understand electroweak symmetry breaking. Third, these new particles often “automatically” have all the right properties to be dark matter. For example, their stability often follows as a result of discrete symmetries that are necessary to make electroweak theories viable, independent of cosmology. And fourth, these new particles are naturally produced with the cosmological densities required of dark matter.

The last motivation is particularly tantalizing. Dark matter may be produced in a simple and predictive manner as a thermal relic of the Big Bang. The evolution of a thermal relic’s number density is shown in Fig. 3. In stage (1), the early Universe is dense and hot, and all particles are in thermal (chemical) equilibrium. In stage (2), the Universe cools to temperatures  $T$  below the dark matter particle’s mass  $m_\chi$ , and the number of dark matter particles becomes Boltzmann suppressed, dropping exponentially as  $e^{-m_\chi/T}$ . In stage (3), the Universe becomes so cold and dilute that the dark matter annihilation rate is too low to maintain equilibrium. The dark matter particles then “freeze out,” with their number asymptotically approaching a constant, their thermal relic density.

More detailed analysis shows that the thermal relic density is rather insensitive to  $m_\chi$  and inversely proportional to the annihilation cross section:  $\Omega_{\text{DM}} \sim \langle \sigma_A v \rangle^{-1}$ . The constant of proportionality depends on the details of the microphysics, but we may give a rough estimate. On dimensional grounds, the cross section can be written

$$\sigma_A v = k \frac{4\pi\alpha_1^2}{m_\chi^2} (1 \text{ or } v^2) , \quad (6)$$

where  $v$  is the relative velocity of the annihilating particles, the factor  $v^2$  is absent or present for  $S$ - or  $P$ -wave annihilation, respectively, and terms higher-order in  $v$  have been neglected. The constant  $\alpha_1$  is the hypercharge fine structure constant, and  $k$  parameterizes deviations from this estimate.

With this parametrization, given a choice of  $k$ , the relic density is determined as a function of  $m_\chi$ . The results are shown in Fig. 3. The width of the band comes from considering both  $S$ - and  $P$ -wave annihilation, and from letting  $k$  vary from  $\frac{1}{2}$  to 2. We see that a particle that makes up all of dark matter is predicted to have mass in the range  $m_\chi \sim 100 \text{ GeV} - 1 \text{ TeV}$ ; a particle that makes up 10% of dark matter, still significant (with respect to its impact on structure formation, for example), has mass  $m_\chi \sim 30 \text{ GeV} - 300 \text{ GeV}$ . There are

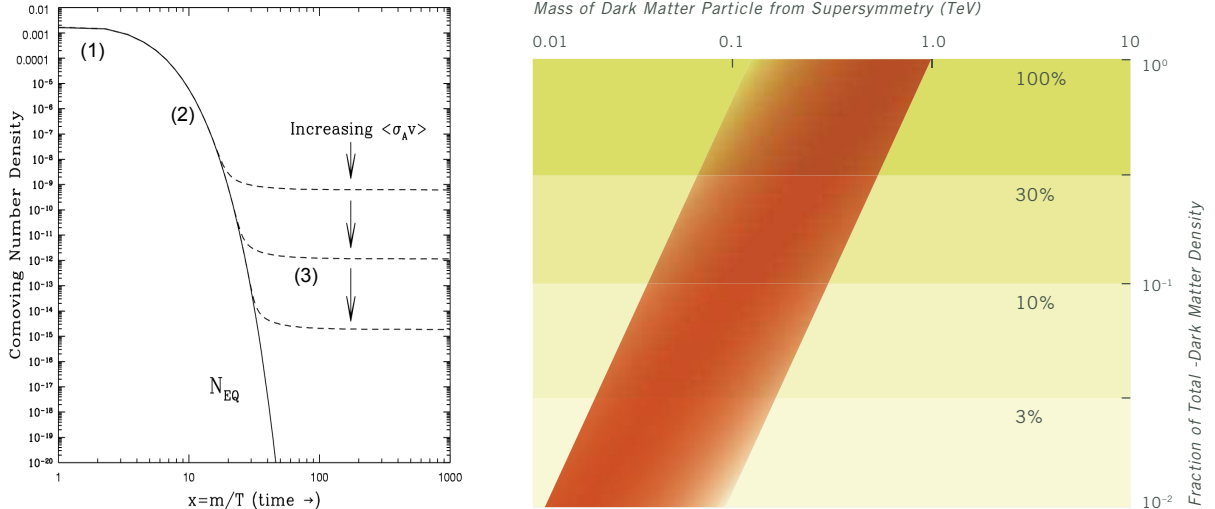


FIG. 3: Left: The cosmological evolution of a thermal relic’s comoving number density. Right: A band of natural values in the  $(m_\chi, \Omega_\chi)$  plane for a thermal relic [34].

models in which the effective  $k$  is outside our illustrative range. In fact, values of  $k$  smaller than we have assumed, predicting smaller  $m_\chi$ , are not uncommon, as the masses of virtual particles in annihilation diagrams can be significantly higher than  $m_\chi$ . In any case, the general conclusion remains: particles with mass at the Fermi scale naturally have significant thermal relic densities. For this reason, a thorough exploration of the Fermi scale is crucial if we hope to identify the particle or particles that make up dark matter. Even null results from LHC and ILC searches for dark matter are important, as without them, it is unlikely that we will be able to exclude the possibility of dark matter at the Fermi scale.

Given these results, many theories for new physics at the Fermi scale contain promising dark matter candidates. The candidates that exploit the tantalizing numerical “coincidence” shown in Fig. 3 may be grouped into two classes: WIMPs and superWIMPs. In the following sections, we consider each of these two cases.

### III. WIMPS

Weakly-interacting massive particles (WIMPs) have weak-scale masses and weak-scale interactions. They are an especially well-motivated class of dark matter particles, and there are many examples, including neutralinos in supersymmetry [21, 22], Kaluza-Klein particles in theories with universal extra dimensions [28, 29], branons in theories with large extra dimensions [30, 31], and the lightest  $T$ -odd particle in some little Higgs theories [35].

A program of detailed WIMP dark matter studies may be divided into three (overlapping) stages:

1. WIMP Candidate Identification. Is there evidence for WIMPs at colliders from, for example, events with missing energy and momentum? Are there signals in dark matter search experiments? What are the candidates’ masses, spins, and other quantum numbers?
2. WIMP Relic Density Determination. What are the dark matter candidates’ predicted

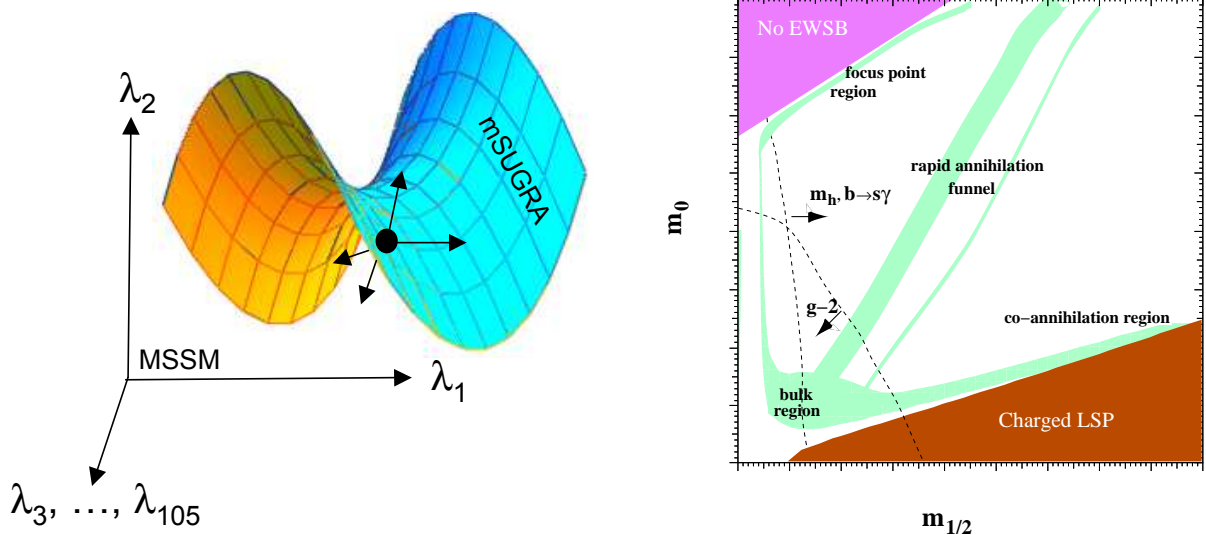


FIG. 4: Left: Minimal supergravity (mSUGRA) defines a hypersurface in the 105-dimensional parameter space of the MSSM. In the studies described here, the underlying parameters are assumed to lie on the mSUGRA hypersurface, but deviations in all directions of the MSSM parameter space are allowed when evaluating the potential of colliders to constrain parameters. Right: Schematic diagram of regions with the right amount of dark matter (shaded) in mSUGRA. This diagram is qualitative. The precise locations of the shaded regions depend on suppressed parameters, and axis labels are purposely omitted [36].

thermal relic densities? Can they be significant components or all of dark matter?

3. Mapping the WIMP Universe. Combining collider results with results from direct and indirect dark matter searches, cosmological observations, and  $N$ -body simulations, what can we learn about astrophysical questions, such as structure formation and the distribution of dark matter in the Universe?

Stage 1 is discussed in Ref. [36]. In the following sections, we will explore how well near future experiments may advance Stages 2 and 3.

To address these issues concretely, it is necessary to focus on one representative example. We choose to study neutralinos. Even with this restriction, there are many qualitatively different scenarios. A common choice is to study minimal supergravity (mSUGRA), a simple model framework that encompasses many different possibilities. In this case, one assumes that the underlying supersymmetry parameters realized in nature are those of a point in mSUGRA parameter space. In determining the capabilities of experiments, however, it is best to relax all mSUGRA assumptions and ask how well the 105 parameters of the general Minimal Supersymmetric Standard Model (MSSM) may be determined. This approach is illustrated in Fig. 4.

In much of mSUGRA parameter space the neutralino relic density lies above the narrow allowed window, and so these possibilities are cosmologically excluded. The regions in which the neutralino relic density is not too large, but is still sufficient to be all of dark matter, are cosmologically preferred. They have been given names and include the bulk, focus point, co-annihilation, and rapid annihilation funnel regions shown in Fig. 4. Results from representative models in each of the first two regions are summarized below. For results for

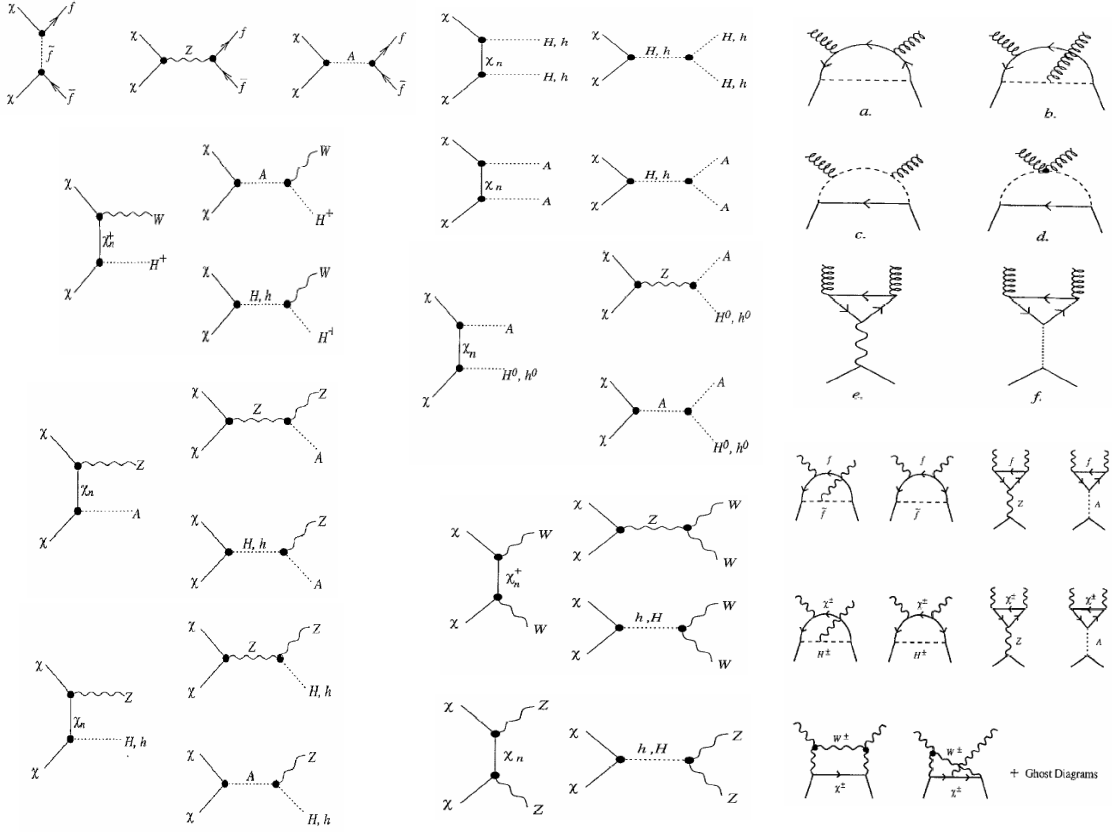


FIG. 5: Processes contributing to neutralino WIMP annihilation [45].

the other two regions and related studies, see Refs. [37, 38, 39, 40, 41]. For each model, the superpartner spectrum is determined by the computer code ISAJET [42], and cosmological observables, such as the thermal relic density, are determined by the software packages DARKSUSY [43] and micrOMEGAs [44].

### A. WIMP Relic Density Determination

To determine the predicted WIMP thermal relic density, one must experimentally constrain all processes contributing significantly to the WIMP pair annihilation cross section. This requires detailed knowledge not only of WIMPs and their properties, but also of all other particles contributing to their annihilation. This is no small task — the number of processes contributing to WIMP annihilation is large, as illustrated in Fig. 5. All unknown parameters at the Fermi scale must be either measured precisely or constrained sufficiently so that their effects are known to be irrelevant. Such detailed work relies primarily on particle colliders, and we now consider how well colliders may constrain the thermal relic density.



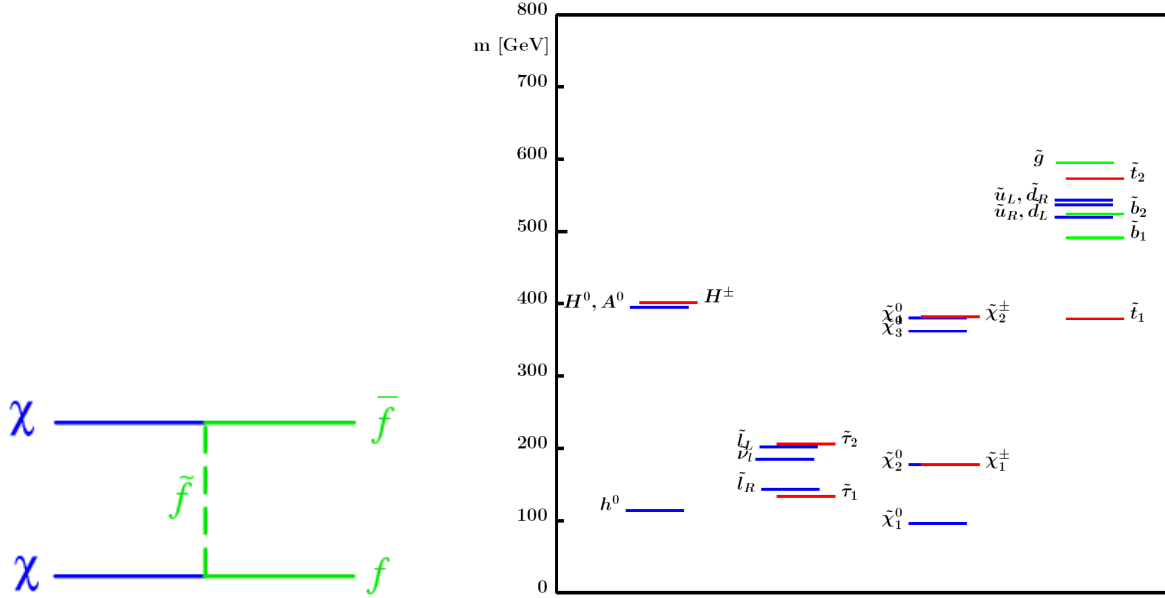


FIG. 6: Left: The dominant neutralino annihilation process in the bulk region. Right: The superpartner spectrum at LCC1, a representative model in the bulk region [46].

### 1. Bulk Region

In the bulk region, a much studied model is specified by the mSUGRA parameters of Linear Collider Cosmology Model 1 (LCC1):

$$\text{LCC1: } (m_0, M_{1/2}, A_0, \tan \beta) = (100 \text{ GeV}, 250 \text{ GeV}, -100 \text{ GeV}, 10), \quad (7)$$

with  $\mu > 0$ ,  $m_{3/2} > m_{\text{LSP}}$ , and  $m_t = 178 \text{ GeV}$ . Here  $m_0$ ,  $M_{1/2}$ , and  $A_0$  are the universal scalar, gaugino, and trilinear coupling masses specified at the grand unified scale  $M_{\text{GUT}} \simeq 2.4 \times 10^{16} \text{ GeV}$ , respectively,  $\tan \beta \equiv \langle H_u^0 \rangle / \langle H_d^0 \rangle$  is the ratio of Higgs boson vacuum expectation values,  $\mu$  is the supersymmetric Higgs mass, and  $m_{3/2}$  is the gravitino mass. The neutralino thermal relic density at this point is  $\Omega_\chi h^2 = 0.19$  ( $h \simeq 0.71$ ), significantly higher than the range  $\Omega_\chi h^2 = 0.113 \pm 0.009$  allowed by the latest cosmological constraints [2, 3]. Nevertheless, the choice of LCC1 is convenient, since it has been studied in great detail in other studies, where it is also known as Snowmass Points and Slopes Model 1a (SPS1a) [46].

In the bulk region, neutralinos annihilate dominantly through  $\chi\chi \rightarrow f\bar{f}$  through a  $t$ -channel scalar  $\tilde{f}$ , as shown in Fig. 6. To achieve the correct relic density, this process must be efficient, requiring light sfermions and, since the neutralino must be the lightest supersymmetric particle (LSP), light neutralinos. These characteristics are exhibited in the superpartner spectrum of LCC1, shown in Fig. 6. It is noteworthy that in this case, cosmology provides a strong motivation for light superpartners within the reach of a 500 GeV ILC.

To determine the relic density at LCC1, all of the supersymmetry parameters entering annihilation processes, including those shown in Fig. 6 and others, must be determined to high accuracy. The LCC1 superpartner spectrum makes possible many high precision measurements at the LHC. LCC1 (SPS1a) is in significant respects a “best case scenario”

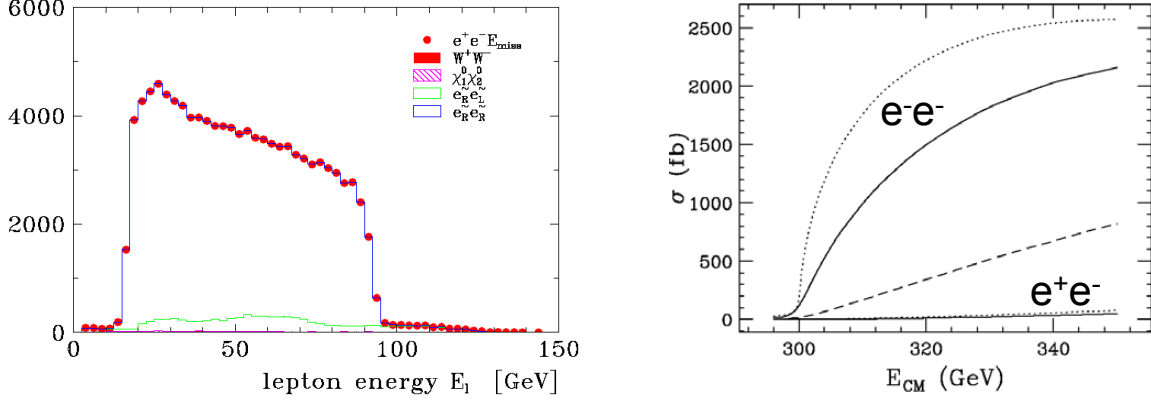


FIG. 7: Left: The kinematic endpoints of lepton energies from  $e^+e^- \rightarrow \tilde{l}^+\tilde{l}^- \rightarrow l^+l^-\chi\chi$  provide precise determinations of slepton and neutralino masses [47]. Right: Threshold scans may also be used to determine slepton masses. In the case of selectron masses,  $e^-e^-$  threshold scans provide higher precision and simultaneously *save* luminosity [48].

for the LHC. The implications of these measurements for cosmology will be summarized below.

The LHC results may be improved at the ILC. For example, superpartner masses may be determined with extraordinary precision through kinematic endpoints and threshold scans, as shown in Fig. 7. The kinematic endpoints of final state leptons in the process  $e^+e^- \rightarrow \tilde{l}^+\tilde{l}^- \rightarrow l^+l^-\chi\chi$  determine both  $\tilde{l}$  and  $\chi$  masses. Slepton masses may also be determined through threshold scans. Threshold scans provide even higher precision, and may actually *save* luminosity. This is the case, for example, for selectron mass determinations through  $e^-e^-$  threshold scans, where precisions of tens of MeV may be obtained with 1 to 10 fb $^{-1}$  of integrated luminosity [48, 49, 50]. More generally, the required measurements exploit the full arsenal of the ILC, from its variable beam energy, to its polarized beams, to the  $e^-e^-$  option. The results of one study are summarized in Fig. 8.

The neutralino thermal relic density may be determined by combining the precise determination of all relevant supersymmetry parameters and also verifying the insensitivity of the relic density to all other parameters. The results depend somewhat on the prescription one uses to combine these data. One approach is to choose points in parameter space at random, weighting each with a Gaussian distribution for each observable. The relic density allowed region is then identified as the symmetric interval around the central value that contains 68% of the weighted probability.

The result of applying this method with 50,000 model parameter points randomly selected around LCC1 is shown in Fig. 9. The result is that the ILC may determine the thermal relic density to a fractional uncertainty of

$$\text{LCC1 (preliminary): } \frac{\Delta(\Omega_\chi h^2)}{\Omega_\chi h^2} = 2.2\% \quad [\Delta(\Omega_\chi h^2) = 0.0042]. \quad (8)$$

The current constraint from WMAP and the projected future constraint from the Planck satellite are also shown. WMAP and Planck provide no information about the mass of the dark matter particle.

	$m$ [GeV]	$\Delta m$ [GeV]	Comments
$\tilde{\chi}_1^\pm$	176.4	0.55	simulation threshold scan, 100 fb <sup>-1</sup>
$\tilde{\chi}_2^\pm$	378.2	3	estimate $\tilde{\chi}_1^\pm \tilde{\chi}_2^\mp$ , spectra $\tilde{\chi}_2^\pm \rightarrow Z \tilde{\chi}_1^\pm, W \tilde{\chi}_1^0$
$\tilde{\chi}_1^0$	96.1	0.05	combination of all methods
$\tilde{\chi}_2^0$	176.8	1.2	simulation threshold scan $\tilde{\chi}_2^0 \tilde{\chi}_2^0$ , 100 fb <sup>-1</sup>
$\tilde{\chi}_3^0$	358.8	3 – 5	spectra $\tilde{\chi}_3^0 \rightarrow Z \tilde{\chi}_{1,2}^0, \tilde{\chi}_2^0 \tilde{\chi}_3^0, \tilde{\chi}_3^0 \tilde{\chi}_4^0$ , 750 GeV, > 1000 fb <sup>-1</sup>
$\tilde{\chi}_4^0$	377.8	3 – 5	spectra $\tilde{\chi}_4^0 \rightarrow W \tilde{\chi}_1^\pm, \tilde{\chi}_2^0 \tilde{\chi}_4^0, \tilde{\chi}_3^0 \tilde{\chi}_4^0$ , 750 GeV, > 1000 fb <sup>-1</sup>
$\tilde{e}_R$	143.0	0.05	$e^-e^-$ threshold scan, 10 fb <sup>-1</sup>
$\tilde{e}_L$	202.1	0.2	$e^-e^-$ threshold scan 20 fb <sup>-1</sup>
$\tilde{\nu}_e$	186.0	1.2	simulation energy spectrum, 500 GeV, 500 fb <sup>-1</sup>
$\tilde{\mu}_R$	143.0	0.2	simulation energy spectrum, 400 GeV, 200 fb <sup>-1</sup>
$\tilde{\mu}_L$	202.1	0.5	estimate threshold scan, 100 fb <sup>-1</sup> [36]
$\tilde{\tau}_1$	133.2	0.3	simulation energy spectra, 400 GeV, 200 fb <sup>-1</sup>
$\tilde{\tau}_2$	206.1	1.1	estimate threshold scan, 60 fb <sup>-1</sup> [36]
$\tilde{t}_1$	379.1	2	estimate $b$ -jet spectrum, $m_{\min}()$ , 1TeV, 1000 fb <sup>-1</sup>

FIG. 8: The precision with which superpartner masses may be determined at the ILC for charginos  $\tilde{\chi}^\pm$ , neutralinos  $\tilde{\chi}^0$ , sleptons  $\tilde{l}$ , and top squark  $\tilde{t}_1$ . The first column gives the underlying value of the masses, the second the constraint from collider studies, and the third the method used to achieve the constraint [47].

## 2. Focus Point Region

In the focus point region, one may choose the representative model, Linear Collider Cosmology Model 2, specified by

$$\text{LCC2: } (m_0, M_{1/2}, A_0, \tan \beta) = (3280 \text{ GeV}, 300 \text{ GeV}, 0, 10) , \quad (9)$$

with  $\mu > 0$ ,  $m_{3/2} > m_{\text{LSP}}$ ,  $m_t = 175 \text{ GeV}$ . In focus point supersymmetry [51, 52], squarks and sleptons are very heavy, and so the diagrams that are dominant in the bulk region are suppressed.<sup>1</sup> Nevertheless, the desired relic density may be achieved [54], because in the focus point region, the neutralino is not a pure Bino, but contains a significant Higgsino component. The processes  $\chi\chi \rightarrow W^+W^-$ , shown in Fig. 10, and  $\chi\chi \rightarrow ZZ$ , which are negligible in the bulk region, therefore become efficient. Neutralino mixing is typically achieved when neutralinos and charginos are fairly light and not too split in mass, and so the demands of neutralino dark matter motivate supersymmetry with light neutralinos and charginos.

Determination of the thermal relic density in the focus point region requires precise measurements of neutralino and chargino masses and their mixings. Applying the method described above for converting collider constraints to a constraint on the thermal relic density, the thermal relic density may be determined with fractional uncertainty

$$\text{LCC2 (preliminary): } \frac{\Delta(\Omega_\chi h^2)}{\Omega_\chi h^2} = 2.4\% \quad [\Delta(\Omega_\chi h^2) = 0.0026] . \quad (10)$$

<sup>1</sup> As a result of this property, models like focus point supersymmetry may be challenging for supersymmetry discovery and study at the LHC [53].

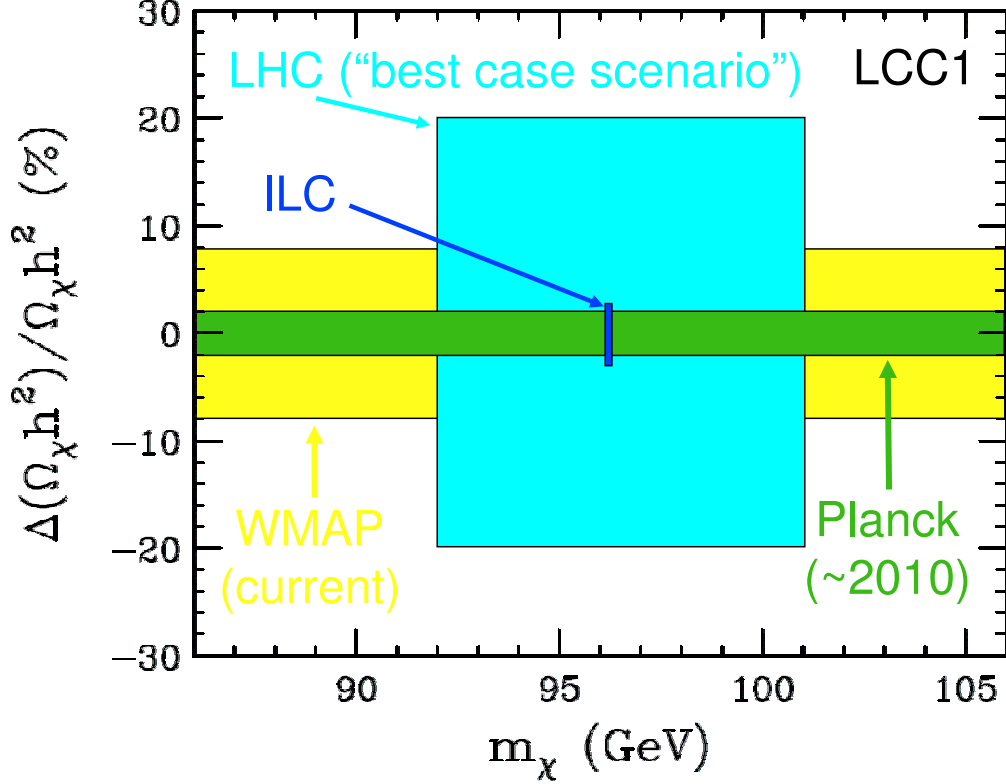


FIG. 9: Constraints in the  $(m_\chi, \Delta(\Omega_\chi h^2)/\Omega_\chi h^2)$  plane from the ILC and LHC. Constraints on  $\Delta(\Omega_\chi h^2)/\Omega_\chi h^2$  from the WMAP and Planck satellite experiments are also shown. The satellite experiments provide no constraints on  $m_\chi$ .

### 3. What We Learn

The results of Figs. 9 and 10 imply that the ILC will provide a part per mille determination of  $\Omega_\chi h^2$  in these cases, matching WMAP and even the extraordinary precision expected from Planck. The many possible implications of such measurements are outlined in the flowchart of Fig. 11.

Consistency of the ILC and WMAP/Planck measurements at the part per mille level would provide strong evidence that neutralinos are absolutely stable and form all of the non-baryonic dark matter. Such a result would at last provide convincing evidence that we have produced dark matter at colliders and that we have identified its microphysical properties. It would be a landmark success of the particle physics/cosmology connection, and would give us confidence in our understanding of the Universe back to neutralino freeze out at  $t \sim 10^{-8}$  s, eight orders of magnitude earlier than can currently be claimed.

On the other hand, inconsistency would lead to a Pandora's box of possibilities, all with important implications. If the thermal relic density determined from high energy physics is smaller than what is required cosmologically, these high precision measurements imply that neutralinos are at most only one component of cold, non-baryonic dark matter. On the other hand, if the thermal relic density determined at colliders is too large, these measurements imply that neutralinos must decay (perhaps to superWIMPs — see below), or that the neutralino thermal relic density is diluted by entropy production or some other effect after

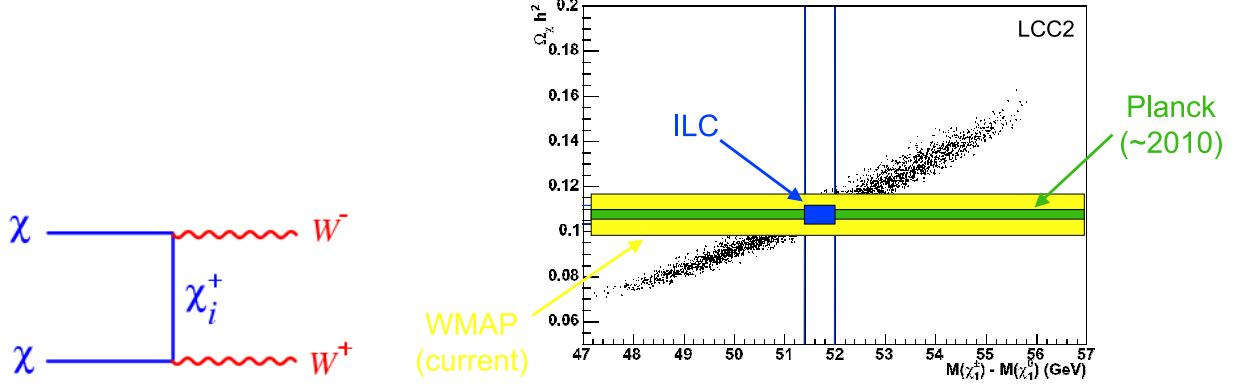


FIG. 10: Left: The dominant neutralino annihilation process in the focus point region. Right: Constraints in the  $(m_\chi, \Omega_\chi)$  plane from the ILC, with constraints on  $\Omega_\chi$  from the WMAP and Planck satellite experiments. The 50,000 scan points used to determine the ILC constraint are also shown (see text) [36]. Note that the distribution of scan points is much broader than the final ILC constrained region; out-lying points have very little probability weight.

freeze out.

The implications of LHC precision measurements for the relic density, determined in the way discussed above, are also shown in Fig. 9. The LHC precision in the LCC1 scenario is extraordinary and unusual; for other scenarios, the LHC is unlikely to determine  $\Omega_\chi$  to better than one or more orders of magnitude. At the same time, even in this “best case scenario,” the LHC determination of  $\Omega_\chi$  leaves open many possibilities. For example, comparison of the LHC result with WMAP/Planck cannot differentiate between a Universe with only neutralino dark matter and a Universe in which dark matter has two components, with neutralinos making up only 80%. Such scenarios are qualitatively distinct, in the sense that the possibility of another component with such significant energy density can lead to highly varying conclusions about the contents of the Universe and the evolution of structure that formed the galaxies we see today.

## B. Mapping the WIMP Universe

WIMPs may appear not only at colliders, but also in dark matter searches. Direct dark matter search experiments look for the recoil of WIMPs scattering off highly shielded detectors. Indirect dark matter searches look for the products, such as positrons, gamma rays or neutrinos, of WIMPs annihilating nearby, such as in the halo, the galactic center, or the core of the Sun.

If WIMPs are discovered at colliders and their thermal relic densities are determined to be cosmologically significant, it is quite likely that they will also be discovered through direct and indirect dark matter search experiments. The requirement of the correct relic density implies that WIMP annihilation was efficient in the early Universe. This suggests efficient annihilation now, corresponding to significant indirect detection rates, and efficient scattering now, corresponding to significant direct detection rates. This rough correspondence is illustrated in Fig. 12.

Direct and indirect dark matter detection rates are subject to uncertainties from both particle physics, through the microphysical properties of dark matter, and astrophysics,

# IDENTIFYING DARK MATTER

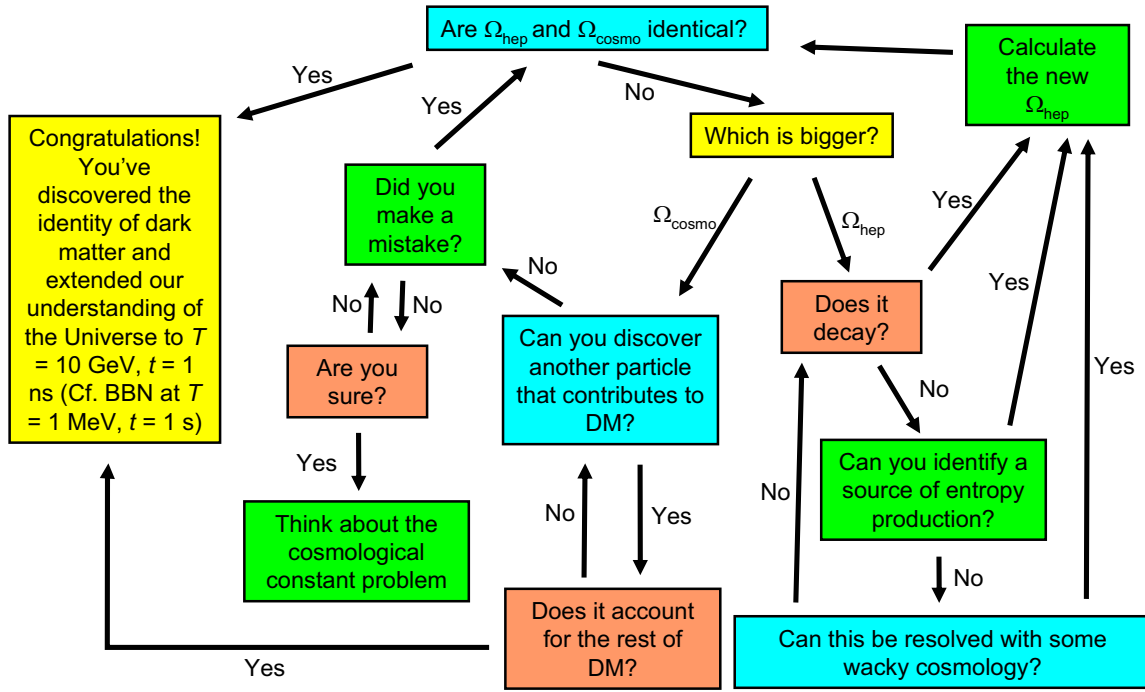


FIG. 11: Flowchart illustrating the possible implications of comparing  $\Omega_{\text{hep}}$ , the predicted dark matter thermal relic density determined from high energy physics, and  $\Omega_{\text{cosmo}}$ , the actual dark matter relic density determined by cosmological observations.

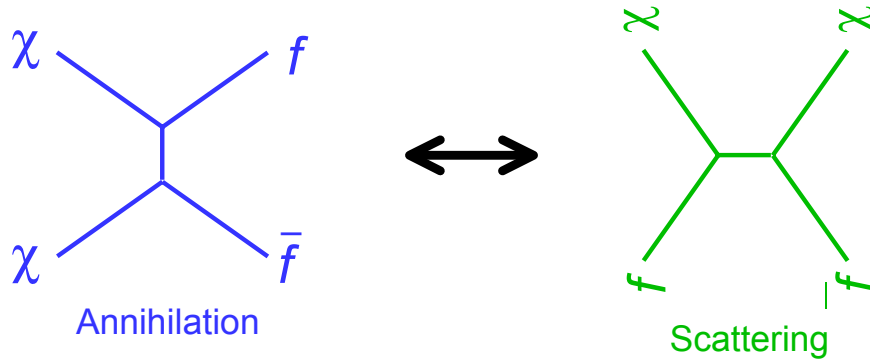


FIG. 12: Efficient annihilation, corresponding to large indirect detection rates, is related to efficient scattering, corresponding to large direct detection rates.

through the spatial and velocity distributions of dark matter. If completed, the research program described in Sec. III A to pin down the properties of WIMPs will effectively remove particle physics uncertainties. Dark matter search experiments then become probes of dark matter distributions.

As an example, consider direct detection. Theoretical predictions of direct detection rates

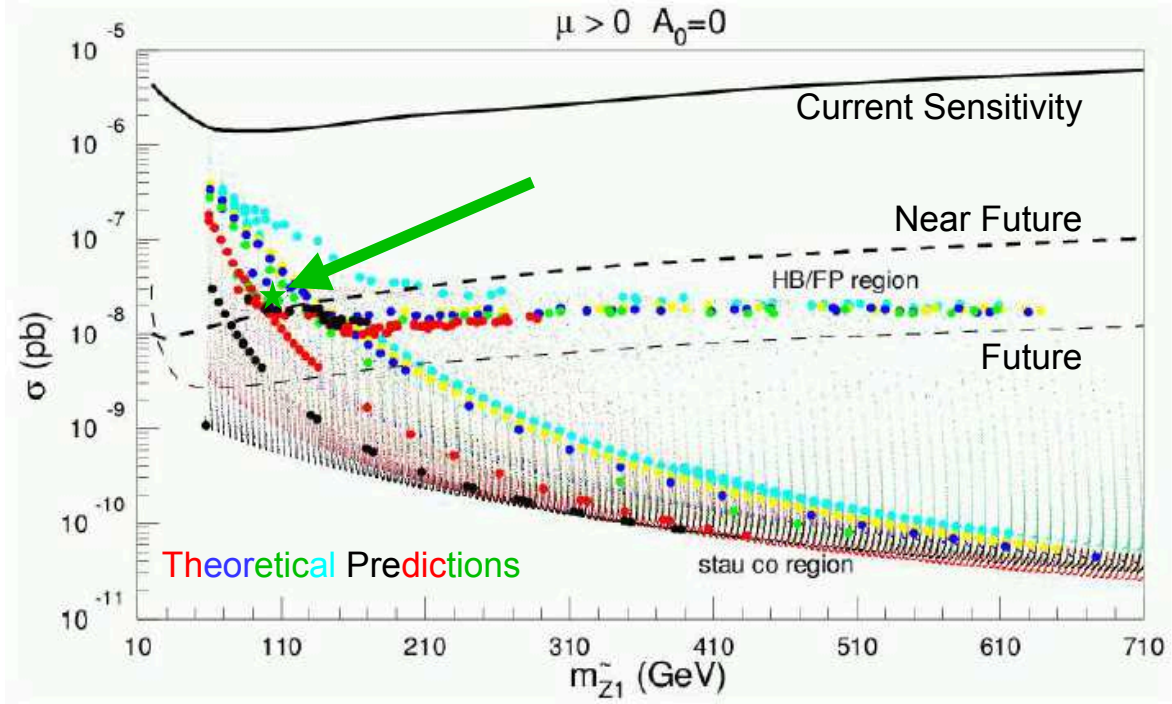


FIG. 13: Theoretical predictions for the direct detection neutralino-proton scattering cross section  $\sigma$ , as a function of neutralino mass  $m_{\tilde{Z}_1} = m_\chi$ , for various mSUGRA models (dots) [55], and the prediction of LCC2 ( $\star$ ). ILC studies will constrain the values of  $\sigma$  and  $m_\chi$  to be smaller than the extent of the  $\star$  plotting symbol [36].

are given in Fig. 13. As is typically done in particle physics studies, a simple dark matter halo profile is assumed throughout this figure. The enormous variation in rates results from particle physics uncertainties alone. LHC and ILC studies will reduce this uncertainty drastically. For example, for LCC2, the dark matter mass will be determined to a GeV at the ILC, and the cross section for neutralino-proton scattering will be determined to  $\Delta\sigma/\sigma \lesssim 10\%$  [36]. This constraint is shown in Fig. 13, where the uncertainties are smaller than the extent of the  $\star$  plotting symbol.

Once collider constraints effectively remove microphysical uncertainties, the direct detection rates give us information about the local dark matter density and velocity profile. In a similar way, indirect detection rates will provide additional complementary information. For example, experiments such as HESS and GLAST may detect photons from dark matter annihilation in the galactic center. Such rates are sensitive to the halo profile at the galactic center, a quantity of great interest at present. The synergy between collider experiments and these dark matter experiments will constrain the phase space distribution of WIMP dark matter in the Universe. Together with  $N$ -body simulations, semi-analytical analyses of galaxy formation, and cosmology observations, these data will have important implications for the formation and evolution of structure.

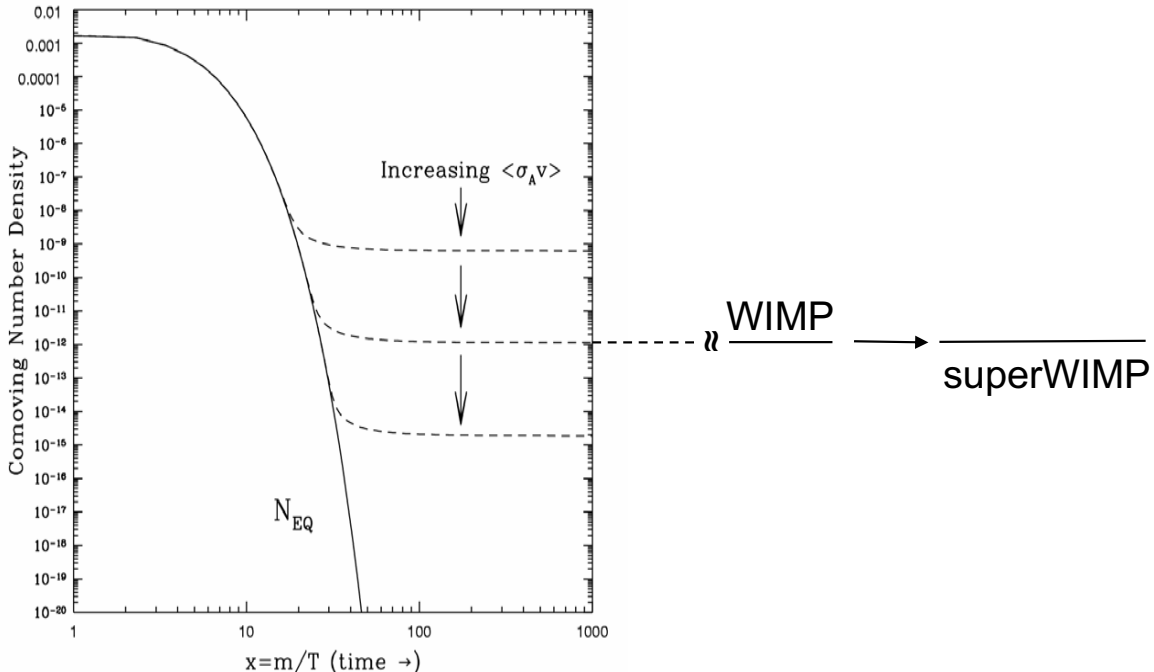


FIG. 14: In superWIMP scenarios, a WIMP freezes out as usual, but then decays to a superWIMP, a superweakly-interacting particle that forms dark matter.

#### IV. SUPERWIMPS

In superWIMP scenarios [32, 33], a WIMP freezes out as usual, but then decays to a stable dark matter particle that interacts *superweakly*, as shown in Fig. 14. The prototypical example of a superWIMP is a weak-scale gravitino produced non-thermally in the late decays of a weakly-interacting next-to-lightest supersymmetric particle (NLSP), such as a neutralino, charged slepton, or sneutrino [32, 33, 56, 57, 58, 59, 60, 61]. Additional examples include axinos [23, 62] and quintessinos [63] in supersymmetry, Kaluza-Klein graviton and axion states in models with universal extra dimensions [64], and stable particles in models that simultaneously address the problem of baryon asymmetry [65]. SuperWIMPs have all of the virtues of WIMPs. They exist in the same well-motivated frameworks and are stable for the same reasons. In addition, in many cases the WIMP and superWIMP masses have the same origin. In these cases, the decaying WIMP and superWIMP naturally have comparable masses, and superWIMPs also are automatically produced with relic densities of the desired order of magnitude.

As noted above, superWIMPs exist in many different contexts. We concentrate here on the case of gravitino superWIMPs. In the simplest supersymmetric models, supersymmetry is transmitted to standard model superpartners through gravitational interactions, and supersymmetry is broken at a high scale. The mass of the gravitino  $\tilde{G}$  is

$$m_{\tilde{G}} = \frac{F}{\sqrt{3}M_*} , \quad (11)$$



and the masses of standard model superpartners are

$$\tilde{m} \sim \frac{F}{M_*} , \quad (12)$$

where  $M_* = (8\pi G_N)^{-1/2} \simeq 2.4 \times 10^{18}$  GeV is the reduced Planck scale and  $F \sim (10^{11} \text{ GeV})^2$  is the supersymmetry breaking scale squared. The precise ordering of masses depends on unknown, presumably  $\mathcal{O}(1)$ , constants in Eq. (12). As discussed in Sec. III, most supergravity studies assume that the LSP is a standard model superpartner, such as the neutralino.

The gravitino may be the LSP, however. In supergravity with high-scale supersymmetry breaking, the gravitino has weak scale mass  $M_{\text{weak}} \sim 100$  GeV and couplings suppressed by  $M_*$ . The gravitino's extremely weak interactions imply that it is irrelevant during thermal freeze out. The NLSP therefore freezes out as usual, and if the NLSP is a slepton, sneutrino, or neutralino, its thermal relic density is again  $\Omega_{\text{NLSP}} \sim 0.1$ . However, eventually the NLSP decays to its standard model partner and the gravitino. The resulting gravitino relic density is

$$\Omega_{\tilde{G}} = \frac{m_{\tilde{G}}}{m_{\text{NLSP}}} \Omega_{\text{NLSP}} . \quad (13)$$

In supergravity, where  $m_{\tilde{G}} \sim m_{\text{NLSP}}$ , the gravitino therefore inherits a relic density of the right order to be much or all of non-baryonic dark matter. *The superWIMP gravitino scenario preserves the prime virtue of WIMPs, namely that they give the desired amount of dark matter without relying on the introduction of new, fine-tuned energy scales.*

The superWIMP scenario differs markedly from other gravitino dark matter scenarios [13, 14, 15, 16, 17, 18, 19, 20, 66, 67, 68, 69]. In the earliest proposals, gravitinos were produced thermally at temperatures  $T \sim M_{\text{Pl}}$ , with  $\Omega_{\tilde{G}} \sim 0.1$  obtained by requiring  $m_{\tilde{G}} \sim \text{keV}$ . Such scenarios are disfavored now by the expectation of an intervening era of inflation, which would dilute such a primordial population. After inflation, however, gravitinos may be produced in an era of reheating. In this case,  $\Omega_{\tilde{G}} \sim 0.1$  is obtained for reheat temperatures  $T_{\text{RH}} \sim 10^{10}$  GeV. In contrast to the superWIMP scenario, it is not clear that gravitino production during reheating has testable consequences, other than the existence of cold dark matter itself. In addition, the reheating scenario requires the introduction of a new scale, in contrast to the superWIMP production mechanism, where the relic density is a function of the Fermi and Planck scales only and is naturally in the desired range. It is important to note, however, that the reheating and superWIMP production mechanisms are not mutually exclusive. The current gravitino relic population may have components from both production mechanisms, resulting in a very simple scenario in which dark matter is composed of two populations of particles with different histories and effects on the early Universe [81].

Because superWIMP gravitinos interact only gravitationally, with couplings suppressed by  $M_*$ , they are impossible to detect in conventional direct and indirect dark matter search experiments. At the same time, the extraordinarily weak couplings of superWIMPs imply other testable signals. The NLSP is a weak-scale particle decaying gravitationally and so has a natural lifetime of

$$\frac{M_*^2}{M_{\text{weak}}^3} \sim 10^4 - 10^8 \text{ s} . \quad (14)$$

This decay time, outlandishly long by particle physics standards, implies testable cosmological signals, as well as novel signatures at colliders.

## A. Cosmology

The most sensitive probes of late decays with lifetimes in the range given in Eq. (14) are from Big Bang nucleosynthesis (BBN) and the Planckian spectrum of the cosmic microwave background (CMB). The impact of late decays to gravitinos on BBN and the CMB are determined by only two parameters: the lifetime of NLSP decays and the energy released in these decays. The energy released is quickly thermalized, and so the cosmological signals are insensitive to the details of the energy spectrum and are determined essentially only by the total energy released.

The width for the decay of a slepton to a gravitino is

$$\Gamma(\tilde{l} \rightarrow l\tilde{G}) = \frac{1}{48\pi M_*^2} \frac{m_l^5}{m_{\tilde{G}}^2} \left[ 1 - \frac{m_{\tilde{G}}^2}{m_l^2} \right]^4, \quad (15)$$

assuming the lepton mass is negligible. (Similar expressions hold for the decays of neutralino NLSPs.) This decay width depends on only the slepton mass, the gravitino mass, and the Planck mass. In many supersymmetric decays, dynamics brings a dependence on many supersymmetry parameters. In contrast, as decays to the gravitino are gravitational, dynamics is determined by masses, and so no additional parameters enter. In particular, there is no dependence on left-right mixing or flavor mixing in the slepton sector. For  $m_{\tilde{G}}/m_{\tilde{l}} \approx 1$ , the slepton decay lifetime is

$$\tau(\tilde{l} \rightarrow l\tilde{G}) \simeq 3.6 \times 10^8 \text{ s} \left[ \frac{100 \text{ GeV}}{m_{\tilde{l}} - m_{\tilde{G}}} \right]^4 \left[ \frac{m_{\tilde{G}}}{\text{TeV}} \right]. \quad (16)$$

This expression is valid only when the gravitino and slepton are nearly degenerate, but it is a useful guide and verifies the rough estimate of Eq. (14).

The energy release is conveniently expressed in terms of

$$\xi_{\text{EM}} \equiv \epsilon_{\text{EM}} B_{\text{EM}} Y_{\text{NLSP}} \quad (17)$$

for electromagnetic energy, with a similar expression for hadronic energy. Here  $\epsilon_{\text{EM}}$  is the initial EM energy released in NLSP decay, and  $B_{\text{EM}}$  is the branching fraction of NLSP decay into EM components.  $Y_{\text{NLSP}} \equiv n_{\text{NLSP}}/n_\gamma$  is the NLSP number density just before NLSP decay, normalized to the background photon number density  $n_\gamma = 2\zeta(3)T^3/\pi^2$ . It can be expressed in terms of the superWIMP abundance:

$$Y_{\text{NLSP}} \simeq 3.0 \times 10^{-12} \left[ \frac{\text{TeV}}{m_{\tilde{G}}} \right] \left[ \frac{\Omega_{\tilde{G}}}{0.23} \right]. \quad (18)$$

Once an NLSP candidate is specified, and assuming superWIMPs make up all of the dark matter, with  $\Omega_{\tilde{G}} = \Omega_{\text{DM}} = 0.23$ , the early Universe signals are completely determined by only two parameters:  $m_{\tilde{G}}$  and  $m_{\text{NLSP}}$ .

### 1. BBN Electromagnetic Constraints

BBN predicts primordial light element abundances in terms of one free parameter, the baryon-to-photon ratio  $\eta \equiv n_B/n_\gamma$ . In the past, the fact that the observed D,  $^4\text{He}$ ,  $^3\text{He}$ , and

${}^7\text{Li}$  abundances could be accommodated by a single choice of  $\eta$  was a well-known triumph of standard Big Bang cosmology.

More recently, BBN baryometry has been supplemented by CMB data, which alone yields  $\eta_{10} = \eta/10^{-10} = 6.1 \pm 0.4$  [2]. This value agrees precisely with the value of  $\eta$  determined by D, considered by many to be the most reliable BBN baryometer. However, it highlights slight inconsistencies in the BBN data. Most striking is the case of  ${}^7\text{Li}$ . For  $\eta_{10} = 6.0 \pm 0.5$ , the value favored by the combined D and CMB observations, the standard BBN prediction is [70]

$${}^7\text{Li}/\text{H} = 4.7_{-0.8}^{+0.9} \times 10^{-10} \quad (19)$$

at 95% CL. This contrasts with observations. Three independent studies find

$${}^7\text{Li}/\text{H} = 1.5_{-0.5}^{+0.9} \times 10^{-10} \quad (95\% \text{ CL}) \quad [71] \quad (20)$$

$${}^7\text{Li}/\text{H} = 1.72_{-0.22}^{+0.28} \times 10^{-10} \quad (1\sigma + \text{sys}) \quad [72] \quad (21)$$

$${}^7\text{Li}/\text{H} = 1.23_{-0.32}^{+0.68} \times 10^{-10} \quad (\text{stat} + \text{sys}, 95\% \text{ CL}) \quad [73] \quad (22)$$

where depletion effects have been estimated and included in the last value. Within the published uncertainties, the observations are consistent with each other but inconsistent with the theoretical prediction of Eq. (19), with central values lower than predicted by a factor of 3 to 4.  ${}^7\text{Li}$  may be depleted from its primordial value by astrophysical effects, for example, by rotational mixing in stars that brings Lithium to the core where it may be burned [74, 75], but it is controversial whether this effect is large enough and consistent with the relatively small scatter of observations to reconcile observations with the BBN prediction [73].

We now consider the effects of NLSP decays to gravitinos. For weakly-interacting NLSPs, that is, sleptons, sneutrinos, and neutralinos, the energy released is dominantly deposited in electromagnetic cascades. For the decay times of Eq. (14), mesons decay before they interact hadronically. The impact of EM energy on the light element abundances has been studied in Refs. [76, 77, 78, 79, 80]. The results of Ref. [79] are given in Fig. 15. The shaded regions are excluded because they distort the light element abundances too much. The predictions of the superWIMP scenario for a stau NLSP with  $m_{\tilde{G}}$  and  $m_{\text{NLSP}}$  varying over weak scale parameters are given in Fig. 15 by the grid.

We find that the BBN constraint excludes some weak scale parameters. However, much of the weak scale parameter space remains viable. Note also that, given the  ${}^7\text{Li}$  discrepancy, the best fit is not achieved at  $\xi_{\text{EM}} = 0$ , but rather for  $\tau \sim 3 \times 10^6$  s and  $\xi_{\text{EM}} \sim 10^{-9}$  GeV, where  ${}^7\text{Li}$  is destroyed by late decays without changing the other relic abundances. This point is marked by the circle in Fig. 15. The energy release predicted in the superWIMP scenario naturally includes this region. The  ${}^7\text{Li}$  anomaly is naturally resolved in the superWIMP scenario by a stau NLSP with  $m_{\text{NLSP}} \sim 700$  GeV and  $m_{\tilde{G}} \sim 500$  GeV.

## 2. BBN Hadronic Constraints

Hadronic energy release is also constrained by BBN [82, 83, 84, 85, 86, 87]. In fact, constraints on hadronic energy release are so severe that even subdominant contributions to hadronic energy may provide stringent constraints.

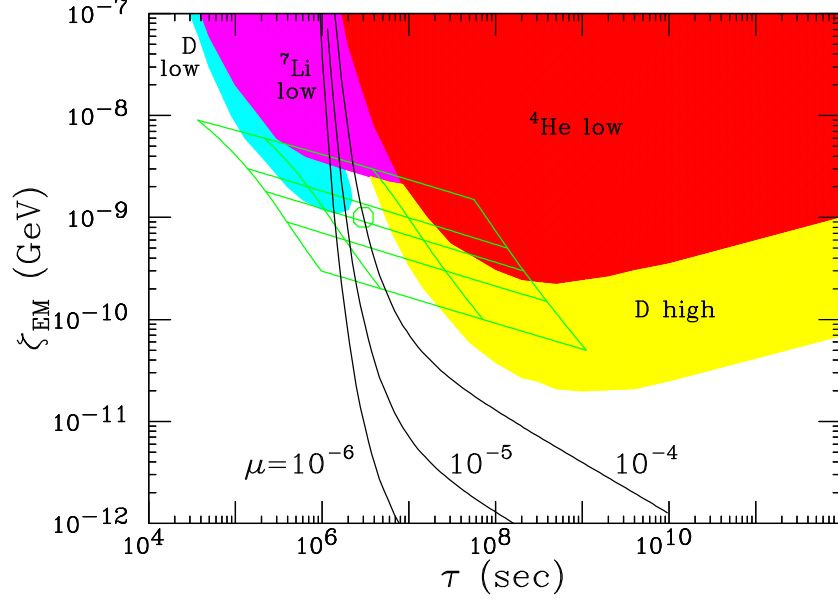


FIG. 15: Predicted and excluded regions of the  $(\tau, \zeta_{\text{EM}})$  plane in the superWIMP dark matter scenario, where  $\tau$  is the lifetime for  $\tilde{l} \rightarrow l\tilde{G}$ , and  $\zeta_{\text{EM}}$  is the normalized electromagnetic energy release. The grid gives predicted values for  $m_{\tilde{G}} = 100 \text{ GeV} - 3 \text{ TeV}$  (top to bottom) and  $\Delta m \equiv m_{\tilde{l}} - m_{\tilde{G}} = 600 \text{ GeV} - 100 \text{ GeV}$  (left to right), assuming  $\Omega_{\tilde{G}} = 0.23$ . BBN constraints exclude the shaded regions; the circle indicates the best fit region where  ${}^7\text{Li}$  is reduced to observed levels without upsetting other light element abundances. Contours of CMB  $\mu$  distortions indicate the current bound ( $\mu < 0.9 \times 10^{-4}$ ) and the expected future sensitivity of Diffuse Microwave Emission Survey (DIMES) ( $\mu \sim 10^{-6}$ ). From Ref. [33].

Slepton and sneutrino decays contribute to hadronic energy through the higher order processes

$$\begin{aligned} \tilde{l} &\rightarrow lZ\tilde{G}, \nu W\tilde{G} \\ \tilde{\nu} &\rightarrow \nu Z\tilde{G}, lW\tilde{G}, \end{aligned} \quad (23)$$

when the  $Z$  or  $W$  decays hadronically. These three-body decays may be kinematically suppressed when  $m_{\tilde{l},\tilde{\nu}} - m_{\tilde{G}} < m_W, m_Z$ , but even in this case, four-body decays, such as  $\tilde{l} \rightarrow l\gamma^*\tilde{G} \rightarrow lq\bar{q}\tilde{G}$ , contribute to hadronic cascades and may be important. The branching fractions for these decays have been calculated in Refs. [57, 58]. The end result is that these constraints are stringent and important, as they exclude regions of parameter space that would otherwise be allowed. At the same time, much of the parameter space in the case of slepton and sneutrino NLSPs remains viable. For details, see Refs. [57, 58].

In contrast to the case of slepton and sneutrino NLSPs, the neutralino NLSP possibility is very severely constrained by bounds on hadronic energy release. This is because neutralinos contribute to hadronic energy even through two-body decays

$$\chi \rightarrow Z\tilde{G}, h\tilde{G}, \quad (24)$$

followed by  $Z, h \rightarrow q\bar{q}$ . The resulting hadronic cascades destroy BBN successes, and exclude this scenario unless such decays are highly suppressed. Kinematic suppression is not viable,

however — if  $m_\chi - m_{\tilde{G}} < m_Z$ , the decay  $\chi \rightarrow \gamma \tilde{G}$  takes place so late that it violates bounds on EM cascades. *Neutralino NLSPs are therefore highly disfavored* [32, 33, 57, 58, 61]; they are allowed only when the two-body decays to  $Z$  and  $h$  bosons are suppressed dynamically, as when the neutralino is photino-like, a possibility that is not well-motivated by high energy frameworks.

### 3. CMB Constraints

The injection of electromagnetic energy may also distort the frequency dependence of the CMB black body radiation [88, 89]. For the decay times of interest, with redshifts  $z \sim 10^5$  to  $10^7$ , the resulting photons interact efficiently through  $\gamma e^- \rightarrow \gamma e^-$  and  $eX \rightarrow eX\gamma$ , where  $X$  is an ion, but photon number is conserved, since double Compton scattering  $\gamma e^- \rightarrow \gamma\gamma e^-$  is inefficient. The spectrum therefore relaxes to statistical but not thermodynamic equilibrium, resulting in a Bose-Einstein distribution function

$$f_\gamma(E) = \frac{1}{e^{E/(kT)+\mu} - 1} , \quad (25)$$

with chemical potential  $\mu \neq 0$ .

In Fig. 15 we show contours of chemical potential  $\mu$ , as determined by updating the analysis of Ref. [88]. (For a more recent analysis and its implications for superWIMPs, see Ref. [89].) The current bound is  $\mu < 9 \times 10^{-5}$  [90, 91]. We see that, although there are at present no indications of deviations from black body, current limits are already sensitive to the superWIMP scenario, and are even beginning to probe regions favored by the BBN considerations described above. In the future, the Absolute Radiometer for Cosmology, Astrophysics, and Diffuse Emission (ARCADE) and Diffuse Microwave Emission Survey (DIMES) experiments may improve sensitivities to  $\mu \approx 2 \times 10^{-6}$  [92]. ARCADE and DIMES will therefore probe further into superWIMP parameter space, and will effectively probe all of the favored region where the  $^7\text{Li}$  underabundance is explained by decays to superWIMPs.

## B. Colliders

The study of superWIMP dark matter at colliders has elements in common with the study of WIMPs, but with key differences. It may also be divided into three (overlapping) stages:

1. SuperWIMP Candidate Identification. Is there evidence for late decays to superWIMPs from collider studies?
2. SuperWIMP Relic Density Determination. What are the superWIMP candidates' predicted relic densities? Can they be significant components or all of dark matter? What are their masses, spins, and other quantum numbers?
3. Mapping the SuperWIMP Universe. Combined with other astrophysical and cosmological results, what can collider studies tell us about astrophysical questions, such as the distribution of dark matter in the Universe?

For Stage 1, collider evidence for superWIMPs may come in one of two forms. Collider experiments may find evidence for charged, long-lived particles. Given the stringent bounds on charged dark matter, such particles presumably decay, and their decay products may be superWIMPs. Alternatively, colliders may find seemingly stable WIMPs, but the WIMP relic density studies described in Sec. III A may favor a relic density that is too large, a conundrum that may be resolved by postulating that WIMPs decay. These two possibilities are not mutually exclusive. In fact, the discovery of charged long-lived particles with too-large predicted relic density is a distinct possibility and would provide strong motivation for superWIMP dark matter.

In the following subsections, we will explore how well the LHC and ILC may advance Stages 2 and 3.

### C. Relic Density Determination

SuperWIMPs are produced in the late decays of WIMPs. Their number density is therefore identical to the WIMP number density at freeze out, and so, as noted in Eq. (13), the superWIMP relic density is

$$\Omega_{\text{superWIMP}} = \frac{m_{\text{WIMP}}}{m_{\text{superWIMP}}} \Omega_{\text{WIMP}} . \quad (26)$$

To determine the superWIMP relic density, we must therefore determine the superWIMP's mass. This is not easy, since the WIMP lifetime may be very large, implying that superWIMPs are typically produced long after the WIMPs have escaped collider detectors.

For concreteness, consider the case of supersymmetry with a stau NLSP decaying to a gravitino superWIMP. (Recall that, if superWIMPs are produced in sufficient numbers to be much of the dark matter, neutralino NLSPs are heavily disfavored, as their late decays invariably violate constraints from BBN and the CMB [32, 33, 57, 58, 61].) As discussed above, the stau's lifetime is outlandishly long by particle physics standards. This gravitino superWIMP scenario therefore implies that the signal of supersymmetry at colliders will be meta-stable sleptons with lifetimes of days to months. Given their large mass, some of these sleptons will be slow, and so will produce highly-ionizing tracks that should be spectacularly obvious at the LHC [93, 94, 95, 96].

At the same time, because some sleptons will be slowly moving and highly-ionizing, they may be trapped and studied [97, 98, 99, 100]. As an example, sleptons may be trapped in water tanks placed outside collider detectors. These water tanks may then be drained periodically to underground reservoirs where slepton decays may be observed in quiet environments. This possibility has been studied in Ref. [98] and is illustrated in Fig. 16. Alternatively, sleptons may be trapped in the detectors themselves [97, 98], or may be stopped in the surrounding rock [100].

How many sleptons may be stopped in a reasonably sized trap? The answer is highly model-dependent. The results for one model with 219 GeV sleptons is shown in Fig. 16. At the LHC, hundreds of sleptons may be caught each year in a 10 kton trap, assuming a luminosity of  $100 \text{ fb}^{-1}/\text{yr}$ . A 10 kton trap is not particularly bulky. The optimal shape is one that covers as much solid angle as possible and is only  $\sim 1 \text{ m}$  thick [98]. These LHC results may be improved significantly if long-lived NLSP sleptons are kinematically accessible at the ILC. For the identical case with 219 GeV sleptons,  $\mathcal{O}(1000)$  sleptons may be trapped each year in a 10 kton trap at the ILC, assuming  $300 \text{ fb}^{-1}/\text{yr}$ . By considering the slightly more general possibility of placing lead or other dense material between the ILC detector and the

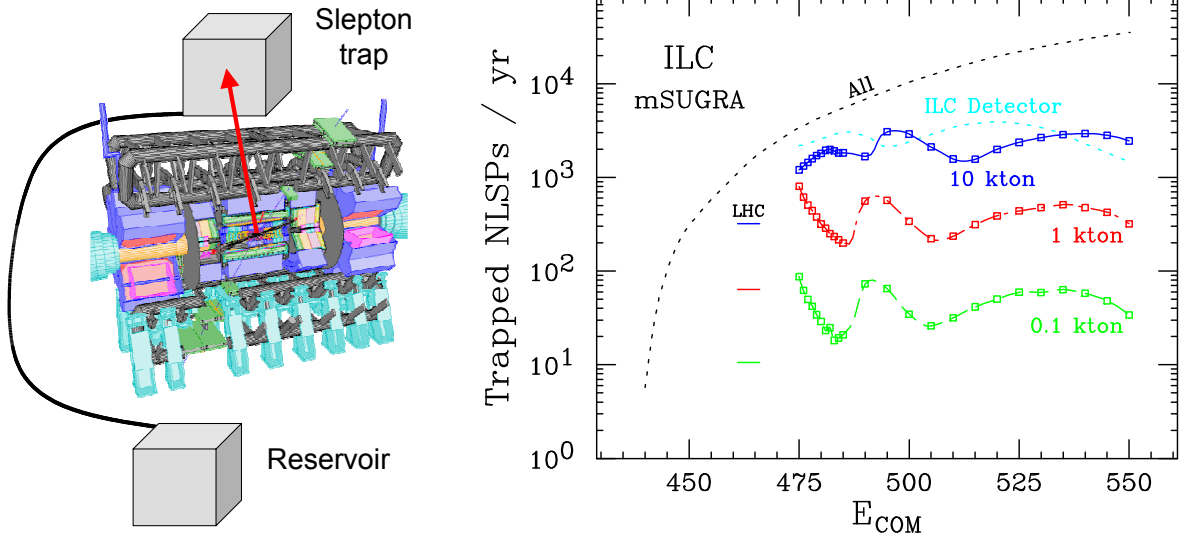


FIG. 16: Left: Configuration for slepton trapping in gravitino superWIMP scenarios. Right: The number of sleptons trapped per year at the ILC in 10 kton (solid), 1 kton (dot-dashed), and 0.1 kton (dashed) water traps. The total number of sleptons produced is also shown (upper dotted) along with the number of sleptons trapped in the ILC detector (lower dotted). The trap shape and placement have been optimized and a luminosity of  $300 \text{ fb}^{-1}/\text{yr}$  is assumed. The underlying model is minimal supergravity with  $M_{1/2} = 600 \text{ GeV}$ ,  $m_0 = 0$ ,  $A_0 = 0$ ,  $\tan \beta = 10$ , and  $\mu > 0$ . The LHC results for this model are as indicated [98].

slepton trap, a further enhancement of an order of magnitude may be possible, allowing up to  $\mathcal{O}(10^4)$  sleptons to be trapped per ILC year. These ILC results are made possible by the ability to tune the beam energy to produce slow NLSPs. The ability to prepare initial states with well-known energies and the flexibility to tune this energy are well-known advantages of the ILC. Here, these features are exploited in a qualitatively new way to produce slow sleptons that are easily captured.

If thousands of sleptons are trapped, the slepton lifetime may be determined to the few percent level simply by counting the number of slepton decays as a function of time. The slepton mass will be constrained by analysis of the collider event kinematics. A percent level measurement of the slepton lifetime given in Eq. (15) therefore implies a high precision measurement of the gravitino mass, and therefore a determination of the gravitino relic density through Eq. (26). As with the case of WIMPs, consistency at the percent level with the observed dark matter relic density will provide strong evidence that dark matter is indeed composed of gravitino superWIMPs.

SuperWIMP quantum numbers and couplings may also be determined through collider studies [101, 102], although, as indicated above, these will typically be determined after or at the same time as the relic density determination, in contrast to the case of WIMPs. For example, an alternative method to determine the gravitino mass is to measure the energy of slepton decay products. This provides a consistency check of the mass determination described above. Alternatively, these two methods, when combined, determine not only  $m_{\tilde{G}}$ , but also the Planck mass  $M_*$ . Given enough events, the gravitino spin may also be constrained to be  $3/2$  through detailed analyses of angular distributions [101], and the gravitino differentiated from other superWIMP candidates, such as the axino [99]. The spin

and couplings of the gravitino may therefore be determined, showing that the superWIMP is in fact the superpartner of the graviton and that nature is locally supersymmetric.

#### D. Mapping the SuperWIMP Universe

Collider studies of superWIMPs will have significant implications for the phase space distribution of dark matter. In fact, the discovery of superWIMPs may resolve current discrepancies and shed light on important and controversial issues in structure formation.

In the standard cosmology, dark matter is assumed to be cold, as is the case with WIMP dark matter. Cold dark matter is remarkably successful in explaining the observed large scale structure down to length scales of  $\sim 1$  Mpc. Despite its considerable virtues, however, cold dark matter appears to face difficulty in explaining the observed structure on length scales  $\lesssim 1$  Mpc. Numerical simulations assuming cold dark matter predict, for example, overdense cores in galactic halos [103] and too many dwarf galaxies in the Local Group [104].

These problems may be alleviated or resolved by superWIMP dark matter [105, 106, 107, 108, 109]. SuperWIMPs are produced with relativistic velocities at late times, as we have seen. They therefore exhibit properties typically associated with warm dark matter, suppressing power on small scales and potentially resolving the problems of cold dark matter mentioned above.<sup>2</sup> The discovery of superWIMP dark matter and the determination of NLSP and superWIMP masses and other relevant parameters at colliders would therefore change fundamentally our understanding of how galaxies were formed and provide a new framework for understanding halo profiles and the distribution of dark matter.

As discussed above, decays that produce superWIMPs also typically release electromagnetic and hadronic energy. This energy may modify the light element abundances predicted by standard BBN [32, 33, 79, 80, 86, 87] or distort the black body spectrum of the CMB [32, 33, 88, 89, 90]. Collider studies will be able to determine how much energy is released and at what time, providing still more information with important consequences for astrophysics and cosmology.

## V. CONCLUSIONS

This is an exciting time at the boundary of particle physics and cosmology. While important microphysical questions related to electroweak symmetry breaking and flavor remain, breakthroughs in cosmology have added a whole new layer of fundamental problems requiring particle physics answers.

Many of the key problems revolve around the mysteries of dark matter. Although there are many viable proposals, we have considered particularly well-motivated candidates whose relic densities are tied to two known energy scales, the Fermi and Planck scales, and fall “coincidentally” in the desired range. There are two classes of dark matter candidates with this property: WIMPs and superWIMPs. In both of these scenarios, dark matter particles, and typically many others, are expected with masses at the Fermi scale  $M_F \sim 100$  GeV. In the next few years, particle colliders will at last probe this scale. If there is new physics,

---

<sup>2</sup> Note that gravitino’s produced thermally during reheating are cold, and do not differ from standard cold dark matter in their impact in structure formation.



experiments at the Tevatron, LHC, and ILC will likely discover it and study it in great detail.

If dark matter is composed of WIMPs, the LHC, and particularly the proposed ILC will be able to determine the WIMP's properties, and may also pin down its thermal relic density. If these determinations match cosmological observations to high precision, then (and only then) we will be able to claim to have determined what dark matter is. Such an achievement will also lead, through synergy with direct and indirect dark matter searches and cosmological observations, to improved knowledge of dark matter distributions and the formation of large scale structure.

If dark matter is composed of superWIMPs, the LHC and ILC will again play a crucial role. The signal of new physics will likely be long-lived charged particles, a spectacular signature that may be evident even in the first year or two of LHC running. By trapping these metastable particles and watching them decay, the properties and relic density of superWIMPs may also be determined, providing another opportunity to identify dark matter. In the superWIMP scenario, the identification of "warm" dark matter may also resolve current issues in structure formation, and will also have implications for Big Bang nucleosynthesis and the cosmic microwave background.

If any of the ideas discussed here is realized in nature, the coming years of exploration will not only provide our first incisive look at the Fermi scale, but will also yield profound insights about the Universe, its contents, and its evolution.

## Acknowledgments

For many contributions to the viewpoints and results summarized here, it is a pleasure to thank James Bullock, Manoj Kaplinghat, Alan Kogut, Ned Wright and the members of the ALCPG Cosmology Subgroup, particularly my co-editors Marco Battaglia, Norman Graf, Michael Peskin, and Mark Trodden and collaborators Jose Ruiz Cembranos, Konstantin Matchev, Arvind Rajaraman, Bryan Smith, Shufang Su, Fumihiro Takayama, and Frank Wilczek. The work of JLF is supported in part by NSF CAREER grant No. PHY-0239817, NASA Grant No. NNG05GG44G, and the Alfred P. Sloan Foundation.

- 
- [1] R. A. Knop *et al.* [The Supernova Cosmology Project Collaboration], *Astrophys. J.* **598**, 102 (2003) [astro-ph/0309368].
  - [2] D. N. Spergel *et al.* [WMAP Collaboration], *Astrophys. J. Suppl.* **148**, 175 (2003) [astro-ph/0302209].
  - [3] M. Tegmark *et al.* [SDSS Collaboration], *Phys. Rev. D* **69**, 103501 (2004) [astro-ph/0310723].
  - [4] T. L. Heath, *A History of Greek Mathematics*, Oxford (1921).
  - [5] B. R. Goldstein, *Historia Math.* **11** (4), 411 (1984).
  - [6] D. Rawlins, *Isis* **73**, 259 (1982).
  - [7] D. Rawlins, *Arch. Hist. Exact Sci.* **26** (3), 211 (1982).
  - [8] E. Gulbekian, *Arch. Hist. Exact Sci.* **37** (4), 359 (1987).
  - [9] See, for example, G. Jungman, M. Kamionkowski and K. Griest, *Phys. Rept.* **267**, 195 (1996) [hep-ph/9506380]; L. Bergstrom, *Rept. Prog. Phys.* **63**, 793 (2000) [hep-ph/0002126]; J. L. Feng, *eConf C0307282*, L11 (2003) [hep-ph/0405215]; *Annals Phys.* **315**, 2 (2005);

- G. Bertone, D. Hooper and J. Silk, Phys. Rept. **405**, 279 (2005) [hep-ph/0404175]; M. Drees, R. Godbole and P. Roy, *Theory and Phenomenology of Sparticles: An Account of Four-dimensional  $N = 1$  Supersymmetry in High Energy Physics*, World Scientific (2004).
- [10] R. D. Peccei and H. R. Quinn, Phys. Rev. D **16**, 1791 (1977).
  - [11] F. Wilczek, Phys. Rev. Lett. **40**, 279 (1978).
  - [12] S. Weinberg, Phys. Rev. Lett. **40**, 223 (1978).
  - [13] H. Pagels and J. R. Primack, Phys. Rev. Lett. **48**, 223 (1982).
  - [14] S. Weinberg, Phys. Rev. Lett. **48**, 1303 (1982).
  - [15] L. M. Krauss, Nucl. Phys. B **227**, 556 (1983).
  - [16] D. V. Nanopoulos, K. A. Olive and M. Srednicki, Phys. Lett. B **127**, 30 (1983).
  - [17] M. Y. Khlopov and A. D. Linde, Phys. Lett. B **138** (1984) 265.
  - [18] J. R. Ellis, J. E. Kim and D. V. Nanopoulos, Phys. Lett. B **145**, 181 (1984).
  - [19] J. R. Ellis, D. V. Nanopoulos and S. Sarkar, Nucl. Phys. B **259**, 175 (1985).
  - [20] R. Juszkiewicz, J. Silk and A. Stebbins, Phys. Lett. B **158**, 463 (1985).
  - [21] H. Goldberg, Phys. Rev. Lett. **50**, 1419 (1983).
  - [22] J. R. Ellis, J. S. Hagelin, D. V. Nanopoulos, K. A. Olive and M. Srednicki, Nucl. Phys. B **238**, 453 (1984).
  - [23] K. Rajagopal, M. S. Turner and F. Wilczek, Nucl. Phys. B **358**, 447 (1991).
  - [24] A. Kusenko and M. E. Shaposhnikov, Phys. Lett. B **418**, 46 (1998) [hep-ph/9709492].
  - [25] D. J. H. Chung, E. W. Kolb and A. Riotto, Phys. Rev. Lett. **81**, 4048 (1998) [hep-ph/9805473].
  - [26] D. N. Spergel and P. J. Steinhardt, Phys. Rev. Lett. **84**, 3760 (2000) [astro-ph/9909386].
  - [27] M. Kaplinghat, L. Knox and M. S. Turner, Phys. Rev. Lett. **85**, 3335 (2000) [astro-ph/0005210].
  - [28] G. Servant and T. M. P. Tait, Nucl. Phys. B **650**, 391 (2003) [hep-ph/0206071].
  - [29] H. C. Cheng, J. L. Feng and K. T. Matchev, Phys. Rev. Lett. **89**, 211301 (2002) [hep-ph/0207125].
  - [30] J. A. R. Cembranos, A. Dobado and A. L. Maroto, Phys. Rev. Lett. **90**, 241301 (2003) [hep-ph/0302041].
  - [31] J. A. R. Cembranos, A. Dobado and A. L. Maroto, Phys. Rev. D **68**, 103505 (2003) [hep-ph/0307062].
  - [32] J. L. Feng, A. Rajaraman and F. Takayama, Phys. Rev. Lett. **91**, 011302 (2003) [hep-ph/0302215].
  - [33] J. L. Feng, A. Rajaraman and F. Takayama, Phys. Rev. D **68**, 063504 (2003) [hep-ph/0306024].
  - [34] HEPAP LHC/ILC Subpanel, “Discovering the Quantum Universe,” <http://www.linearcollider.org>.
  - [35] H. C. Cheng and I. Low, JHEP **0309**, 051 (2003) [hep-ph/0308199].
  - [36] Report of the Cosmology Subgroup, American Linear Collider Physics Group, in preparation.
  - [37] R. Gray *et al.*, hep-ex/0507008.
  - [38] A. Birkedal *et al.*, hep-ph/0507214.
  - [39] M. Battaglia and M. E. Peskin, hep-ph/0509135.
  - [40] B. C. Allanach, G. Belanger, F. Boudjema and A. Pukhov, JHEP **0412**, 020 (2004) [hep-ph/0410091].
  - [41] T. Moroi, Y. Shimizu and A. Yotsuyanagi, Phys. Lett. B **625**, 79 (2005) [hep-ph/0505252].
  - [42] F. E. Paige, S. D. Protopescu, H. Baer and X. Tata, hep-ph/0312045.

- [43] P. Gondolo, J. Edsjo, P. Ullio, L. Bergstrom, M. Schelke and E. A. Baltz, JCAP **0407**, 008 (2004) [astro-ph/0406204].
- [44] G. Belanger, F. Boudjema, A. Pukhov and A. Semenov, hep-ph/0405253.
- [45] These Feynman graphs are presented in the first paper of Ref. [9], and are analyzed in full detail in M. Drees and M. M. Nojiri, Phys. Rev. D **47**, 376 (1993) [hep-ph/9207234]; M. Drees, G. Jungman, M. Kamionkowski and M. M. Nojiri, Phys. Rev. D **49**, 636 (1994) [hep-ph/9306325].
- [46] B. C. Allanach *et al.*, in *Proc. of the APS/DPF/DPB Summer Study on the Future of Particle Physics (Snowmass 2001)* ed. N. Graf, Eur. Phys. J. C **25**, 113 (2002) [eConf **C010630**, P125 (2001)] [hep-ph/0202233].
- [47] G. Weiglein *et al.* [LHC/LC Study Group], hep-ph/0410364.
- [48] J. L. Feng and M. E. Peskin, Phys. Rev. D **64**, 115002 (2001) [hep-ph/0105100].
- [49] J. L. Feng, Int. J. Mod. Phys. A **13**, 2319 (1998) [hep-ph/9803319]; Int. J. Mod. Phys. A **15**, 2355 (2000) [hep-ph/0002055].
- [50] A. Freitas, A. von Manteuffel and P. M. Zerwas, Eur. Phys. J. C **34**, 487 (2004) [hep-ph/0310182].
- [51] J. L. Feng and T. Moroi, Phys. Rev. D **61**, 095004 (2000) [hep-ph/9907319].
- [52] J. L. Feng, K. T. Matchev and T. Moroi, Phys. Rev. Lett. **84**, 2322 (2000) [hep-ph/9908309]; Phys. Rev. D **61**, 075005 (2000) [hep-ph/9909334].
- [53] H. Baer, T. Krupovnickas, S. Profumo and P. Ullio, hep-ph/0507282.
- [54] J. L. Feng, K. T. Matchev and F. Wilczek, Phys. Lett. B **482**, 388 (2000) [hep-ph/0004043]; Phys. Rev. D **63**, 045024 (2001) [astro-ph/0008115].
- [55] H. Baer, C. Balazs, A. Belyaev and J. O’Farrill, JCAP **0309**, 007 (2003) [hep-ph/0305191].
- [56] J. R. Ellis, K. A. Olive, Y. Santoso and V. C. Spanos, Phys. Lett. B **588**, 7 (2004) [hep-ph/0312262].
- [57] J. L. Feng, S. Su and F. Takayama, Phys. Rev. D **70**, 063514 (2004) [hep-ph/0404198].
- [58] J. L. Feng, S. Su and F. Takayama, Phys. Rev. D **70**, 075019 (2004) [hep-ph/0404231].
- [59] F. Wang and J. M. Yang, Eur. Phys. J. C **38**, 129 (2004) [hep-ph/0405186].
- [60] J. R. Ellis, K. A. Olive, Y. Santoso and V. C. Spanos, Phys. Lett. B **603**, 51 (2004) [hep-ph/0408118].
- [61] L. Roszkowski and R. Ruiz de Austri, JHEP **0508**, 080 (2005) [hep-ph/0408227].
- [62] L. Covi, J. E. Kim and L. Roszkowski, Phys. Rev. Lett. **82**, 4180 (1999) [hep-ph/9905212]; L. Covi, H. B. Kim, J. E. Kim and L. Roszkowski, JHEP **0105**, 033 (2001) [hep-ph/0101009]; L. Covi, L. Roszkowski, R. Ruiz de Austri and M. Small, JHEP **0406**, 003 (2004) [hep-ph/0402240].
- [63] X. J. Bi, M. z. Li and X. m. Zhang, Phys. Rev. D **69**, 123521 (2004) [hep-ph/0308218].
- [64] J. L. Feng, A. Rajaraman and F. Takayama, Phys. Rev. D **68**, 085018 (2003) [hep-ph/0307375].
- [65] R. Kitano and I. Low, hep-ph/0503112.
- [66] J. R. Ellis, G. B. Gelmini, J. L. Lopez, D. V. Nanopoulos and S. Sarkar, Nucl. Phys. B **373**, 399 (1992).
- [67] T. Moroi, H. Murayama and M. Yamaguchi, Phys. Lett. B **303**, 289 (1993).
- [68] M. Bolz, A. Brandenburg and W. Buchmuller, Nucl. Phys. B **606**, 518 (2001) [hep-ph/0012052].
- [69] Other production mechanisms for axinos have also been considered in A. Brandenburg and F. D. Steffen, JCAP **0408**, 008 (2004) [hep-ph/0405158].

- [70] S. Burles, K. M. Nollett and M. S. Turner, *Astrophys. J.* **552**, L1 (2001) [astro-ph/0010171].
- [71] J. A. Thorburn, *Astrophys. J.* **421**, 318 (1994).
- [72] P. Bonifacio and P. Molaro, *MNRAS*, **285**, 847 (1997).
- [73] S. G. Ryan, T. C. Beers, K. A. Olive, B. D. Fields and J. E. Norris, *Astrophys. J. Lett.* **530**, L57 (2000) [astro-ph/9905211].
- [74] M. H. Pinsonneault, T. P. Walker, G. Steigman and V. K. Narayanan, *Astrophys. J.* **527**, 180 (1999) [astro-ph/9803073].
- [75] S. Vauclair and C. Charbonnel, *Astrophys. J.* **502**, 372 (1998) [astro-ph/9802315].
- [76] M. Kawasaki and T. Moroi, *Astrophys. J.* **452**, 506 (1995) [astro-ph/9412055].
- [77] E. Holtmann, M. Kawasaki, K. Kohri and T. Moroi, *Phys. Rev. D* **60**, 023506 (1999) [hep-ph/9805405].
- [78] M. Kawasaki, K. Kohri and T. Moroi, *Phys. Rev. D* **63**, 103502 (2001) [hep-ph/0012279].
- [79] R. H. Cyburt, J. R. Ellis, B. D. Fields and K. A. Olive, *Phys. Rev. D* **67**, 103521 (2003) [astro-ph/0211258].
- [80] J. R. Ellis, K. A. Olive and E. Vangioni, *Phys. Lett. B* **619**, 30 (2005) [astro-ph/0503023].
- [81] See, for example, D. G. Cerdeno, K. Y. Choi, K. Jedamzik, L. Roszkowski and R. Ruiz de Austri, hep-ph/0509275.
- [82] M. H. Reno and D. Seckel, *Phys. Rev. D* **37**, 3441 (1988).
- [83] S. Dimopoulos, R. Esmailzadeh, L. J. Hall and G. D. Starkman, *Astrophys. J.* **330**, 545 (1988).
- [84] S. Dimopoulos, R. Esmailzadeh, L. J. Hall and G. D. Starkman, *Nucl. Phys. B* **311**, 699 (1989).
- [85] K. Kohri, *Phys. Rev. D* **64**, 043515 (2001) [astro-ph/0103411].
- [86] K. Jedamzik, *Phys. Rev. D* **70**, 063524 (2004) [astro-ph/0402344].
- [87] M. Kawasaki, K. Kohri and T. Moroi, *Phys. Lett. B* **625**, 7 (2005) [astro-ph/0402490]; *Phys. Rev. D* **71**, 083502 (2005) [astro-ph/0408426].
- [88] W. Hu and J. Silk, *Phys. Rev. Lett.* **70**, 2661 (1993).
- [89] R. Lamon and R. Durrer, hep-ph/0506229.
- [90] D. J. Fixsen, E. S. Cheng, J. M. Gales, J. C. Mather, R. A. Shafer and E. L. Wright, *Astrophys. J.* **473**, 576 (1996) [astro-ph/9605054].
- [91] S. Eidelman *et al.* [Particle Data Group Collaboration], *Phys. Lett. B* **592**, 1 (2004).
- [92] <http://arcade.gsfc.nasa.gov/arcade>; <http://map.gsfc.nasa.gov/DIMES>.
- [93] M. Drees and X. Tata, *Phys. Lett. B* **252**, 695 (1990).
- [94] J. L. Goity, W. J. Kossler and M. Sher, *Phys. Rev. D* **48**, 5437 (1993) [hep-ph/9305244].
- [95] A. Nisati, S. Petrarca and G. Salvini, *Mod. Phys. Lett. A* **12**, 2213 (1997) [hep-ph/9707376].
- [96] J. L. Feng and T. Moroi, *Phys. Rev. D* **58**, 035001 (1998) [hep-ph/9712499].
- [97] K. Hamaguchi, Y. Kuno, T. Nakaya and M. M. Nojiri, *Phys. Rev. D* **70**, 115007 (2004) [hep-ph/0409248].
- [98] J. L. Feng and B. T. Smith, *Phys. Rev. D* **71**, 015004 (2005) [hep-ph/0409278].
- [99] A. Brandenburg, L. Covi, K. Hamaguchi, L. Roszkowski and F. D. Steffen, *Phys. Lett. B* **617**, 99 (2005) [hep-ph/0501287].
- [100] A. De Roeck, J. R. Ellis, F. Gianotti, F. Moortgat, K. A. Olive and L. Pape, hep-ph/0508198.
- [101] W. Buchmuller, K. Hamaguchi, M. Ratz and T. Yanagida, *Phys. Lett. B* **588**, 90 (2004) [hep-ph/0402179].
- [102] J. L. Feng, A. Rajaraman and F. Takayama, *Int. J. Mod. Phys. D* **13**, 2355 (2004) [hep-th/0405248].

- [103] B. Moore, *Nature* **370**, 629 (1994); R. A. Flores and J. R. Primack, *Astrophys. J.* **427**, L1 (1994) [astro-ph/9402004]; J. J. Binney and N. W. Evans, *Mon. Not. Roy. Astron. Soc.* **327**, L27 (2001) [astro-ph/0108505]; A. R. Zentner and J. S. Bullock, *Phys. Rev. D* **66**, 043003 (2002) [astro-ph/0205216]; J. D. Simon *et al.*, *Astrophys. J.* **621**, 757 (2005) [astro-ph/0412035].
- [104] A. A. Klypin, A. V. Kravtsov, O. Valenzuela and F. Prada, *Astrophys. J.* **522**, 82 (1999) [astro-ph/9901240]; A. R. Zentner and J. S. Bullock, *Astrophys. J.* **598**, 49 (2003) [astro-ph/0304292].
- [105] K. Sigurdson and M. Kamionkowski, *Phys. Rev. Lett.* **92**, 171302 (2004) [astro-ph/0311486].
- [106] S. Profumo, K. Sigurdson, P. Ullio and M. Kamionkowski, *Phys. Rev. D* **71**, 023518 (2005) [astro-ph/0410714].
- [107] M. Kaplinghat, *Phys. Rev. D* **72**, 063510 (2005) [astro-ph/0507300].
- [108] J. A. R. Cembranos, J. L. Feng, A. Rajaraman and F. Takayama, *Phys. Rev. Lett.* **95**, 181301 (2005) [hep-ph/0507150].
- [109] K. Jedamzik, M. Lemoine and G. Moulhaka, astro-ph/0508141.